Electric Field Controlled Electrospray Deposition for Precise Particle Pattern and Cell Pattern Formation

Jingwei Xie, Alireza Rezvanpour, and Chi-Hwa Wang
Dept. of Chemical and Biomolecular Engineering, National University of Singapore, Singapore 117576

Jinsong Hua
Institute of High Performance Computing, 1 Fusionopolis Way, 16-16 Connexis, Singapore 138632, Singapore

DOI 10.1002/aic.12198
Published online February 3, 2010 in Wiley Online Library (wileyonlinelibrary.com).

Photolithography, soft lithography, and ink jetting have been used for automated micropattern fabrication. However, most of the methods for microfabrication of surface pattern are limited to the investigation of material properties of substrates with high-cost and complex procedures. In the present study, we show a simple (single-step) yet versatile and robust approach to generate biodegradable polymeric particle patterns on a substrate using electrospray deposition through a mask. Various particle patterns including patterned dots, circles, squares, and bands can be easily formed and the features of particle patterns could also be tailored using different masks and electrostatic focusing effects. Furthermore, cell patterns can be achieved on the surface of particle patterns by blocking the areas without particle deposition on the substrate and culturing cells on the substrate. Polymeric particle patterns and cell patterns developed in this study could be used in the high throughput screening of sustained release formulations, cell-based sensing, and drug discovery. In addition to experimental results, an analysis of the associated electric field is used to investigate quantitatively the nature of focusing effect. Scaling analysis is also applied to obtain the dominate terms in electrospray deposition process.
 AIChE J, 56: 2607–2621, 2010
Keywords: electrospray, deposition, focusing effect, particle pattern, cell pattern, scaling analysis

Introduction

The microarray and micropattern technologies have attracted tremendous interests among researchers owing to their wide applications in the fields of optics, biotechnology, electronics, medical and clinical diagnosis, disease finger printing, drug screening, targeting and evaluation, toxicity assessment, signal transduction study, and cancer treatment development.[1–3] Microfabrication techniques including photolithography, soft lithography, and ink jetting have been widely used for automated micropattern fabrication.[2,3] The details of surface engineering approaches to achieve micropattern surfaces can be referred to the review work by Geissler and Xia.[4] However, most of the methods for microfabrication of surface pattern are limited to material properties of substrates, high cost, and complex procedures. Cell patterning is also an important tool for organizing cells on transducers for cell-based sensing and cell-based drug discovery.[5] In addition, controlling cellular microenvironment using micropatterning may be used in directing cell fate for tissue engineering applications.[6] Cell patterning approaches can also be used to study fundamentals of cell biology such as

Correspondence concerning this article should be addressed to C.-H. Wang at chewch@nus.edu.sg.

cell-ECM interactions and cell–cell interactions.[7] Photolithography is used to pattern a layer of photosensitive polymer by means of light.[8] However, it is limited in its applications to biotechnology because of its high cost, limited control over surface properties, indirect application to proteins and cells, and time consuming from design to prototype.[9–11] Low efficiency of substance transfer, the necessity for new stamp for each substance deposited, and a thorough washing of the same stamp after deposition of each substance can be considered as major drawbacks of soft lithography method.[12] Ink-jet printing pattern materials by depositing microscopic droplets under robotic control in a programmable manner has been used for micropattern generation of cell adhesion materials for defined neuronal adhesion on various substrates.[11,12] In addition, patterning mammalian cells using elastomeric membrane was studied.[13] The main principle of cell patterning is to engineer the surface of a substrate to make one part cell adhesive and the other cell repulsive.

Furthermore, only few studies have reported on micropatterned colloid particles, which were investigated with lithographically patterned electrodes,[13,14] micromoulds,[15] electrical-field-induced colloid particle patterns,[16] field-induced layering of colloid crystals,[17] stick-slip motion of single colloid particle lines,[18] and dewetting-induced self-organization of nanoparticles.[19] Electrospray is a process in which a liquid is forced through a capillary and a potential difference of the order of kilo volts is applied between the capillary and the collection electrode. Electrospray deposition is one of the technologies to fabricate micropatterns and has been used to fabricate protein pattern as biochips. Buchko et al. fabricated microarray using electrospray deposition with a conductive mask where deposition occurs on both mask and substrate evenly, resulting in the loss of raw materials and poor spot density due to lack of focusing effect.[20–23] Although Morozov et al. used a dielectric mask for electrospray deposition, the deposition efficiency was improved comparing to the method by Buchko et al., the interspot distance was still large (1 mm) and it was limited to the dielectric mask and conductive substrate.[24,25] Kim et al. used a dielectric mask and a conductive substrate with a combination of a surface acoustic wave atomizer and electrostatic deposition to fabricate protein chips.[26] However, the major issues as mentioned before still remained.

Electrospray deposition is also a simple and versatile method for generating thin films in a variety of applications including $LiCoO_2$ films, $NiCo_2O_4$ films, ceramic thin films, Nafion films, starch films, protein films, cellulose films, poly (vinylidene fluoride) films, and other organic thin films.[27–37] When combined with the use of a mask, a pattern of deposition substance can be formed on the substrate under the mask, after the mask was lifted off. Morozov and Morozova first demonstrated that electrospray deposition can be used for a simultaneous parallel fabrication of multicomponent arrays from different substances with dots of any form and size ranging from millimeters to micrometers.[13] Subsequently, immobilization of proteins in immunochemical microarrays fabricated by electrospray deposition was developed.[24] Recently, immunoassay with multicomponent protein microarrays was fabricated by electrospray deposition.[25] More recently, coelectrospraying of nanoparticle suspension and ions, such as N_2 ions or Na^+ was reported to create particle arrays on a surface by modifying the applied field to produce electrostatic lenses.[38,39] Most recently, Li et al. and Ahmad et al. examined inorganic hydroxylapatite nanocrystal pattern formation using template-assisted electrohydrodynamic atomization spraying and their potential biomedical applications.[21–23]

In contrast, electrospray deposition has not yet been commonly used to fabricate polymeric particle pattern. In our previous studies, controllable size and morphology of biodegradable polymeric particles were achieved by electrospray approach.[40,41] The aim of this work was to engineer the surface of a substrate through the formation of polymeric particle pattern to extend the application of electrospray deposition by making use of focusing effect due to the presence of extra electrical potential applied to the mask. The issues of traditional electrospray deposition can be solved, such as reducing the loss of raw materials, enhancing deposition efficiency, increasing the spot density, and reducing the large inherent interspot distance. Furthermore, the development of living cell patterns on the surface of the substrate can be realized. The present work would cover the following sections: first, to micropattern pluronic F127 and poly(lactic-*co*-glycolic acid) (PLGA) particles on the surface of substrates using electrospray deposition through a mask without and with assisted electrical potential applied to the mask; second, to micropattern PLGA particles on the surface of substrates coated with pluronic F127 using electrospray deposition through a mask and subsequently culture cells on the surface of substrates to form cell patterns. Finally, to develop a mathematical model by considering force balance and charge conservation equations and assess the relative importance of the various terms in these equations through scaling analysis. The novelty of the study can be briefly described as the integration of theoretical investigation and experimental studies to quantitatively understand the fundamentals of micropattern in electrospray deposition.

Materials and Methods

Materials

Poly (D, L-lactic-*co*-glycolic acid) (PLGA) with L:G molar ratio of 50:50 (MW = 90,000–120,000) was purchased from Sigma Aldrich (St. Louis, MO). Dichloromethane (DCM), dimethylformamide (DMF), ethanol, and acetonitrile were purchased from Tedia Company (Fairfield, OH). Pluronic F127 was obtained from BASF company (Germany). Masks were provided by J A Associates (Singapore). Fluorescein diacetate (FDA) and fluorescein isothiocyanate labeled polystyrene (FITC-PS) nanoparticles used for living cell staining and micropattern formation study were bought from Sigma Aldrich (St. Louis, MO). All other materials and reagents used were of analytical grade.

Particle pattern formation

In this study, 5% of Pluronic F127 in ethanol, 10% of PLGA in acetonitrile, 5% of PLGA in DCM solutions, 20% of PLGA in DMF and fluorescein isothiocyanate labeled polystyrene (FITC-PS) nanoparticles in water and ethanol solution were used for particle pattern fabrication by electrospray deposition through a mask, respectively. A vertical

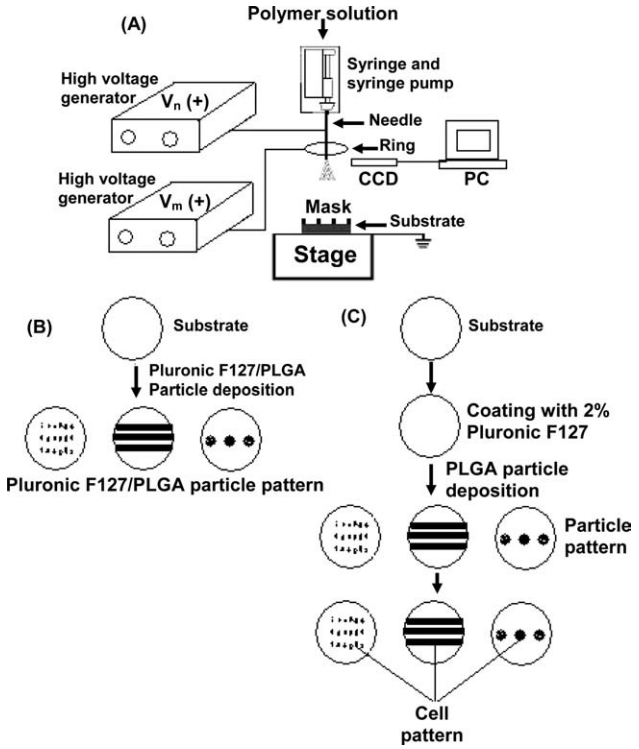

Figure 1. (A) A schematic of electrospray deposition setup; (B) and (C) Schematics showing formation of particle and cell patterns.

geometry was used for particle pattern fabrication as shown in Figure 1A. The capillary was given a voltage (as compared to the ground) of around 5.0 to 10.0 kV, which was sufficient for the solution to reach a stable cone-jet mode for spraying. The metal ring, given a potential difference (as compared with the ground) of 4.0 to 8.0 kV, was used to stabilize the electrospray towards the mounted glass slide. This was necessary since the high viscosity of the polymeric solution often caused partial clogging of the needle (25 Gauge, outer diameter: 0.41 mm), resulting in deviance in spraying direction. The syringe pump (Stoelting, IL) was set from 0.1 to 3.0 ml/h for different samples, and the deposition distance between the tip of the needle and the glass slide was about 2–5 cm. The particle patterns after fabrication were observed by optical microscopy (Leica DMIL) with Nikon Digital Camera DXM1200F.

A slightly different setup was also applied to generate micropatterns using electrospray deposition, which is shown in Figure 2. In this new setup, the ring was removed and an additional electrical potential source was applied to a mask mesh, which controlled the electrical field nearby the substrate and helped to focus the deposited materials on dielectric or conductive substrates. The potential difference between mask and substrate was formed by applying certain positive electrical potential to the conductive mask while the dielectric substrate (glass slide) is electrically grounded. Inversely, it can be implemented by applying negative electrical potential to the conductive substrate while the dielectric mask is electrically grounded. The superposition of electric potential field can result in the focusing effect for controlled deposition. In addition, glass slides can be used as the target substrate for collection, which is especially important for biotechnological applications. For the pluronic F127 coating, the substrate home-made plastic slides were immersed in 2% pluronic F127 in water solution for 24 h and then washed with DI water three times.

SEM imaging

The morphology of particle pattern was observed using scanning electron microscopy (SEM), field emission scanning electron microscopy (FSEM). SEM (Jeol JSM 5600LV, Tokyo, Japan) and FSEM (Jeol JSM, Tokyo, Japan) required an ion coating with platinum by a sputter coater (JFC-1300, Jeol, Tokyo, Japan) for 40 s in a vacuum at a current intensity of 40 mA after preparing the sample on metallic studs with double-sided conductive tape. The accelerating voltage ranged from 5–15 kV during scanning.

Cell patterning formation

Hep G2 cells were grown in DMEM supplemented with 10% fetal bovine serum (FBS), 1% penicillin and streptomycin. Cells were transferred to micropatterned samples or controls at a density of 1×10^5 cells/ml. Cells were incubated for around 3 days, gently rinsed with culture media to remove loosely adherent cells, and imaged under phase-contrast optical microscope. Living cells were stained with Fluorescein Diacetate (FDA) following the standard procedures. Subsequently, cover slips were taken out and samples were observed by fluorescence microscope (Leica DMIL) with Nikon Digital Camera DXM1200F using a 488-nm wavelength filter.

Results and Discussion

Particle pattern formation

Figure 1A shows the schematic drawing of the electrospray deposition setup illustrating the formation of particle patterns. In a typical electrospray procedure, pluronic F127 in ethanol or PLGA in DCM was fed through a needle. The

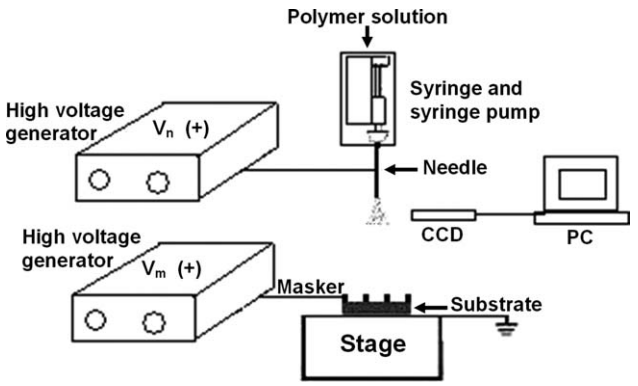

Figure 2. A schematic of modified electrospray deposition setup.

V_n, potential difference between needle tip and the substrate; V_m, potential difference between mask and substrate. The schematic of a mask shows the size of holes is 150 μm $\times$ 150 μm.

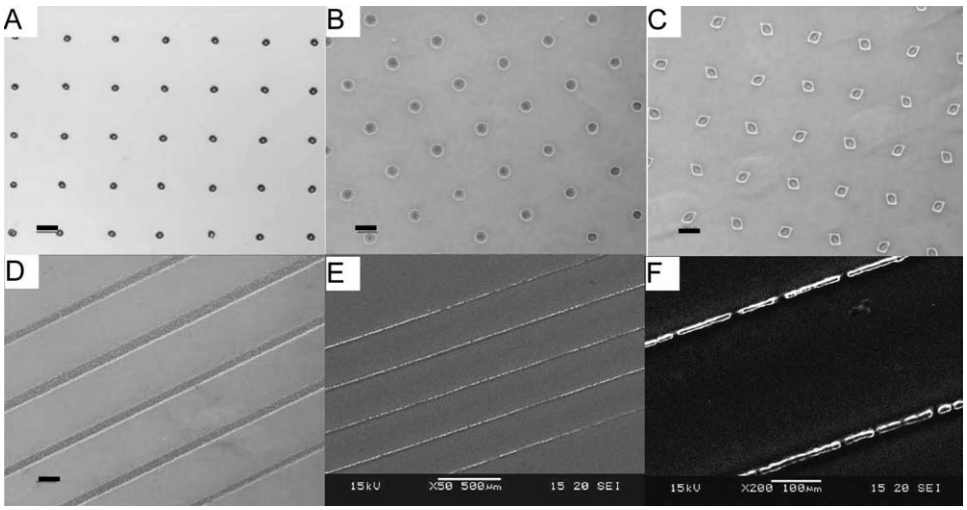

Figure 3. (A–D) Optical microscopy images of various pluronic F127 particle patterns; (E, F) SEM images of pluronic F127 pattern.

These samples were prepared with a feed rate of 0.5 ml/h for 5% (w/v) of pluronic F127 in ethanol solution. (—) scale bar: 100 μm.

feeding rate of the solution was controlled by a syringe pump. Different spray modes including dripping mode, single cone-jet mode, and multiple-cone jet mode can be achieved by altering the high voltage difference between the needle and ground. In the present study, electrospray deposition was operated in the single cone-jet mode, which was used to generate nearly monodispersed droplets. After solvent evaporation from the droplets, solid polymeric particles were formed either before or after reaching the surface of substrate, depending on the distance of deposition. The procedures to form particle pattern and cell pattern by electrospray deposition of polymeric particles through a mask were shown in Figures 1B, C. Various pluronic F127 particle patterns including patterned dots, circles, squares, and bands can be easily formed by electrospray deposition through the use of different masks and the feature size of patterns obtained in this study was around 30–200 μm as shown in Figure 3. The regions of pluronic F127 seemed to shrink after coating with Pt in this SEM observation, which could be due to the effects of coating temperature. Figure 4 shows images of pluronic F127 particle patterns on the substrate and pluronic F127 particles deposited on the surface of a mask. The obtained size for pluronic F127 particles was around 2 μm as shown in Figure 4E. Similar approach may be used to spray other types of particle suspensions in appropriate solvents to generate particle patterns.

Figures 5A–G shows optical microscopy images of a variety of PLGA particle patterns. Furthermore, it is

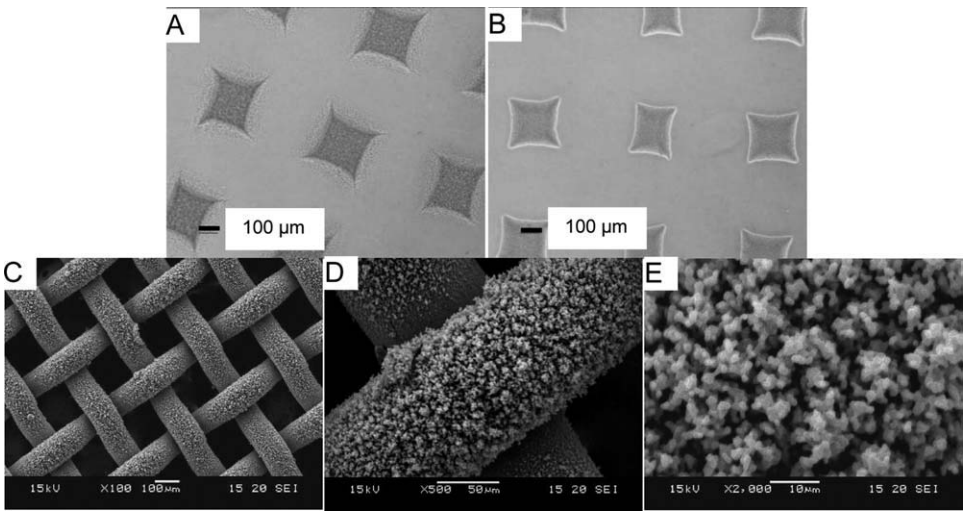

Figure 4. (A, B) Optical images of pluronic F127 pattern; (C, D) SEM images of pluronic F127 particles deposited on the surface of a mask; (E) High-magnification SEM image of (D).

These samples were prepared with a feed rate of 0.5 ml/h for 5% (w/v) of pluronic F127 in ethanol.

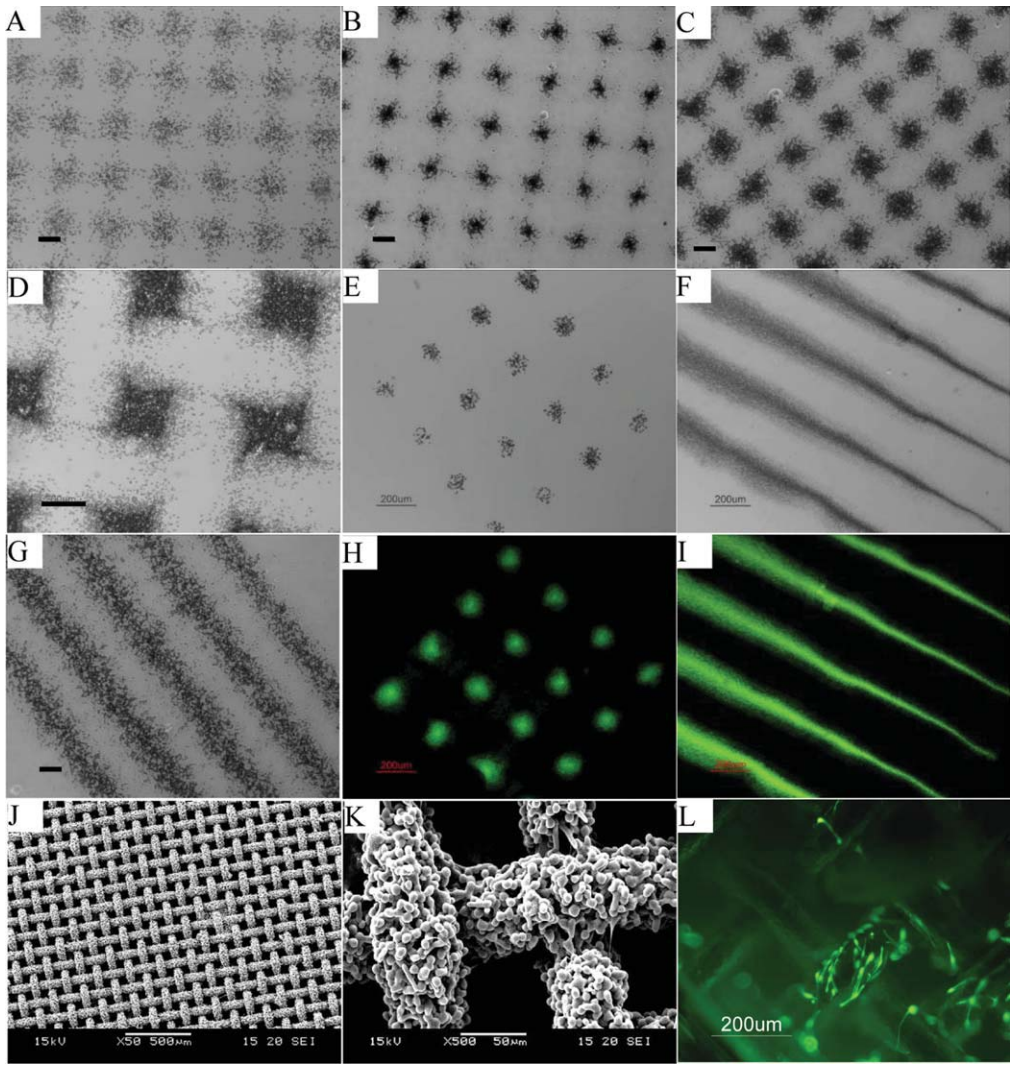

Figure 5. PLGA particle patterns.

(A–G) Optical microscope images of various PLGA particle patterns; (A–C) PLGA particle patterns with different deposition times: 1, 5, 10 min; (H and I): Fluorescent microscope images of coumarin6-loaded PLGA particle patterns; (J and K) SEM images of PLGA particles deposited on the surface of a mask; (L) cell growth on the mask after PLGA particle deposition. These samples were prepared with a feed rate of 3 ml/h for 5% PLGA DCM solution. (—) scale bar for (A–I) and (L): 200 μm. [Color figure can be viewed in the online issue, which is available at wileyonlinelibrary.com.]

demonstrated that coumarin 6-loaded biodegradable polymeric particle patterns can be achieved. Fluorescence microscopy images indicate the distribution of coumarin6 encapsulation inside PLGA particles (in green color) as shown in Figures 5H, I. The encouraging results might be extended to various types of bioactive materials/molecules such as proteins, enzymes, and DNA fragments.[42] These materials/molecules may be loaded inside the biodegradable particles which form the patterns, and could be used for the screening of sustained release formulations, sensing systems, diagnostic systems, or regulate cell fate locally. Moreover, Roh et al. reported that multicomponent particles (biphasic Janus particles and triphasic particles) can be obtained by using electrospray through side-by-side dual or triple capillaries.[43,44] Therefore, the particle patterns with multi components encapsulation could be achieved using a similar approach. Figure 5L shows the fluorescent microscope image of living cells stained with FDA, which grew on the mask after deposition of PLGA particles. This finding suggests that electrospray deposition could be used to engineer the surface by coating the cell-repulsive surface with cell-adhesive materials and vice versa. Figures 6A–C shows SEM images of PLGA particle patterns prepared with a feed rate of 3 ml/h for 5% PLGA DCM solution. The high magnification SEM images corresponding to Figures 6A–C are shown in Figures 6D–F. The organic solvent was partially evaporated before the particles were deposited on the substrate and therefore, the partially dried droplets collapsed and interconnected particles can be observed subsequently. For this case, complete solvent evaporation can be achieved by increasing the distance between the tip of the needle and the substrate. Figures 6G–I shows SEM image of PLGA pattern

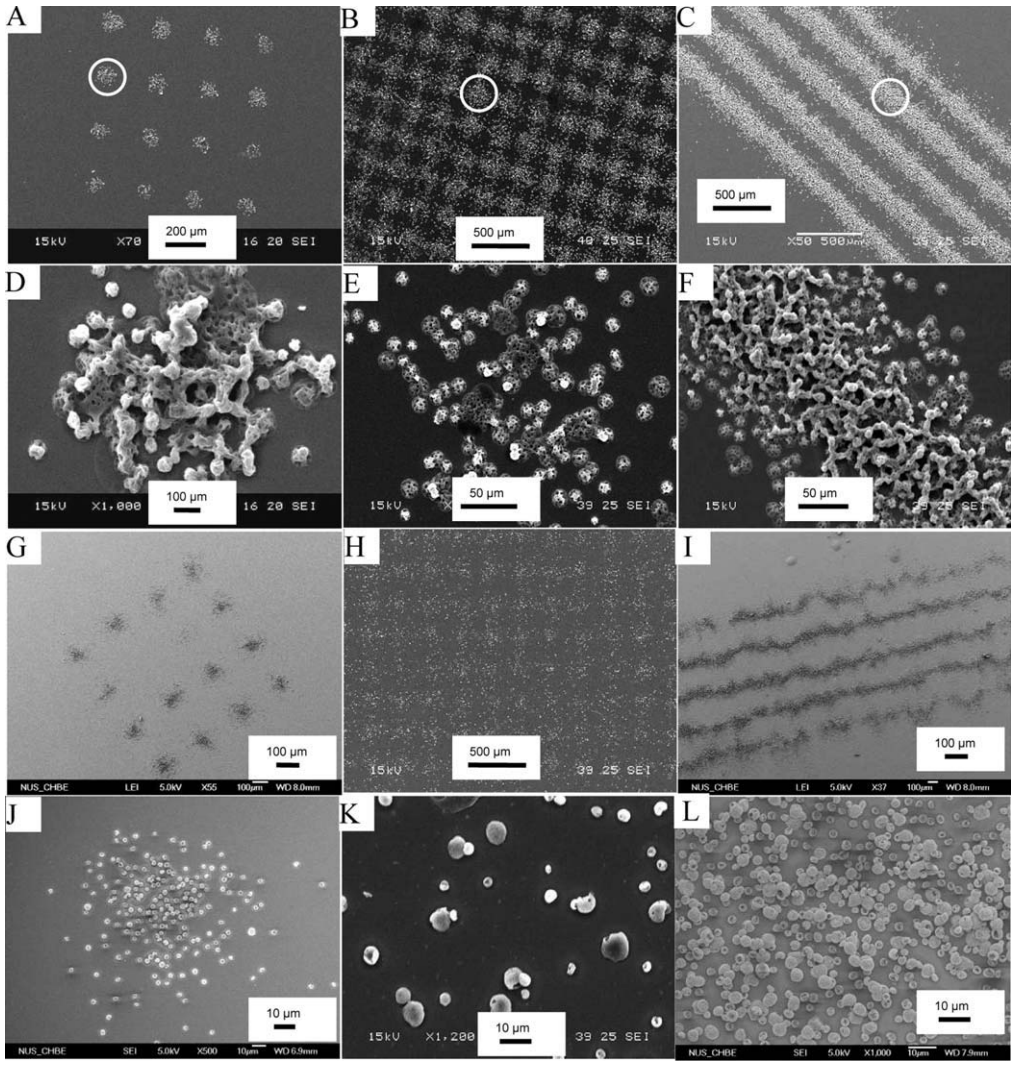

Figure 6. SEM images of PLGA particle patterns.

(A–C) Prepared with a feeding rate of 3 ml/h for 5% PLGA DCM solution; (D–F) High-magnification SEM images for the circular regions labeled in panels A, B, and C, respectively; (G–I) Prepared with a feed rate of 0.5 ml/h for 10% PLGA acetonitrile solution; (J–L) High-magnification SEM image of G, H, and I, respectively.

prepared with a feeding rate of 0.5 ml/h for 10% PLGA acetonitrile solution and discrete particles can be found on the substrate due to the faster acetonitrile evaporation as compared to DCM. It can be observed from Figure 6 that the particle size could be tailored by varying the processing parameters and solution properties, and the size of biodegradable polymeric particle ranging from 200 nm to several tens of microns was reported in our previous studies.[40,41]

For setup shown in Figure 2, the 3D electrical field calculation was used to verify the focusing effect, which was obtained using the software COMSOL3.3 as shown in Figure 7. With an increase of the potential difference between mask and substrate, the focusing effect can be clearly observed. Similar focusing effect was also observed in an inverse arrangement, where a negative high voltage was applied to the conductive substrate and the mask dielectric was grounded. To investigate the focusing effect experimentally, 20% of PLGA in DMF solution was sprayed at the flow rate of 0.2 ml/h under different potential differences (V_m) between mask and substrate. No clear pattern was formed when V_m was set zero. With increasing V_m, the deposition pattern was clearly observed due to the electrical field focusing effect. The focusing effect was also demonstrated experimentally as shown in Figure 7. In addition, the focusing effect was also observed when FITC-PS nanoparticles in ethanol solution were deposited to form patterns as shown in Figure 8. Interestingly, if deposition time is long enough at the flow rate of 0.2 ml/h, the particle deposition controlled by electric field can be self-assembled to form micropatterns with three-dimensional microstructures such as particle-rod as shown in Figures 9A,B. In practice, especially after

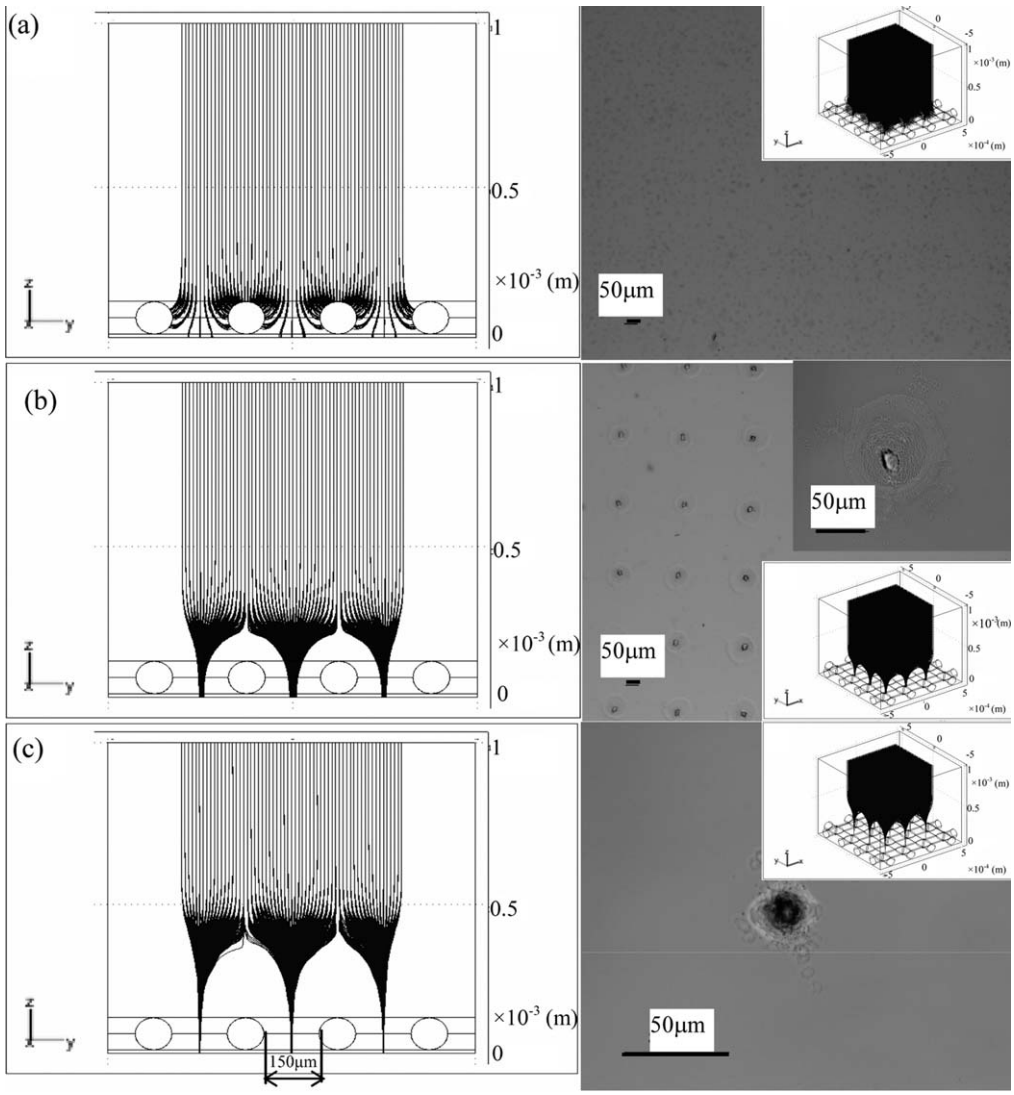

Figure 7. Computational simulation vs. experimental patterns.

Simulated electric field stream lines with a constant voltage 7.5 kV applied to the nozzle are plotted against optical phase contrast images of PLGA patterns under different potential differences between mask and substrate. (a) 0V, (b) 500V, and (c) 2000V. The solution used in electro-spray is 2% PLGA in DMF.

deposition over an extended period of time, some particles could be deposited on the surface of masks and the charges, which particles carried could change the local electric field. The electric field streamline could alter, possibly resulting in dispersed particles around tree-like rod. In addition, the flow rate could also be used to tune micropatterns with different three-dimensional structures. The micropatterns of tree-like branched structures were formed at the flow rat of 0.5 ml/h (inserted picture in Figure 9B) because high liquid flow rate produces large number of particles as to allow high possibility of particle deposition at various points such that growth of the branched structure happens along multiple directions. Different micropatterns could be obtained by replacing different masks and the wall-like PLGA micropattern was obtained as shown in Figures 9C, D. Likewise FITC-PS nanoparticles with the size of 200 nm could be deposited to form a protruding particle cluster at the center. The stronger fluorescence intensity observed at the center position rather than at the peripheral part of the deposited spot was due to the high density of FITC-PS nanoparticles at the center position. Similar 3D microstructure formed by nanoparticles deposition with aerodynamic focusing effect was reported.[45]

Cell pattern formation

Commonly, BSA, PEG-based surface modification materials, and PEO-based tri-block polymers have been used as cell repulsive materials.[46] In the present study, pluronic F127 was chosen as the block material to inhibit cell adhesion. After coating hydrophobic substrate (plastic slides) with pluronic

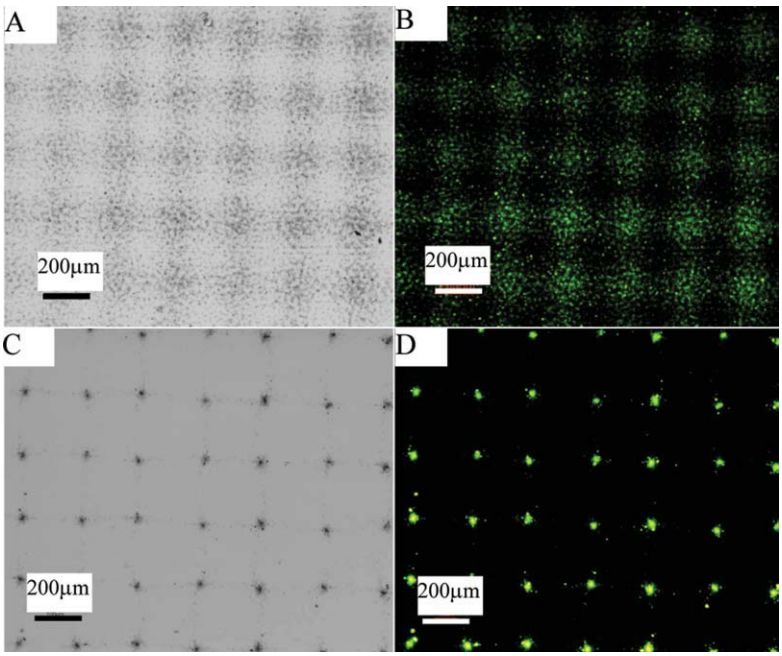

Figure 8. Optical phase contrast (A, C) and fluorescence microscopy (B, D) images of FITC-PS nanoparticle patterns under different potential differences between mask and substrate.

(A, B) 0 V; (C, D) 2000 V. [Color figure can be viewed in the online issue, which is available at wileyonlinelibrary.com.]

F127 to make the regions without particle deposition cell-repulsive, cells were seeded to the particle patterns and cell patterns could be obtained after 3-day incubation with Hep G2 cells as shown in Figure 10. Figures 10A–C shows optical phase contrast images of cell arrays, which were formed on the surface of particle pattern. After FDA staining, fluorescence microscopy images indicate clear cell arrays in green color as shown in Figures 10D–F, which suggest that cells prefer to grow on the surface of PLGA particle patterns. Also, it was observed from Figure 10E that one cluster consisted of ~30 cells. Cell adhesive materials, such as fibronectin and collagen could be sprayed together with polymers to enhance cell adhesive property. The cell pattern shown in Figure 10F is about 10 times larger than Figure 10E. This comparison illustrates the capability of controlling the length scales of different cell patterns by the present study. Figure 10G as one of negative controls shows that the cells did not grow on the surface of PLGA particle pattern, which could be due to the adsorption of pluronic F127 on the surface but grew on the region without PLGA particle deposition on the glass slide substrate. No cell pattern formation was observed on the surface of PLGA particle pattern (on the plastic slide substrate) without coating of pluronic F127 or directly on the plastic slide substrate as shown in Figures 10H, I.

Computational analysis

In addition to experimental results, a mathematical model has been developed to analyze the associated electric field to investigate quantitatively the nature of focusing effect.

Governing Equations. Poisson's equation (Eq. 1) in spherical coordinates is applied to calculate the electrical potential field.

$$\nabla^2 V = \frac{1}{r^2}\frac{\partial}{\partial r}\left(r^2\frac{\partial V}{\partial r}\right) + \frac{1}{r^2\sin\theta}\frac{\partial}{\partial\theta}\left(\sin\theta\frac{\partial V}{\partial\theta}\right) + \frac{1}{r^2\sin^2\theta}\frac{\partial^2 V}{\partial\phi^2} = \frac{-\rho}{\varepsilon_0} \quad (1)$$

where V is the electrical potential, ε_0 is the electrical permittivity of air, and ρ is the space charge density. The electrical field vector, $\mathbf{E}$, for spherical coordinates can then be calculated by taking the negative gradient of the electrical potential field as mentioned in Eq. 2.

$$\mathbf{E} = -\nabla V = -\left(\frac{\partial V}{\partial r}\mathbf{r} + \frac{1}{r}\frac{\partial V}{\partial\theta}\boldsymbol{\theta} + \frac{1}{r\sin\theta}\frac{\partial V}{\partial\phi}\boldsymbol{\varphi}\right) \quad (2)$$

In this equation, $\mathbf{r}$, $\boldsymbol{\theta}$, and $\boldsymbol{\varphi}$ are the unit vectors in r, θ, and φ directions, respectively. The electrical potential is monotonously distributed in θ and φ directions; hence, the related components in Eqs. 1 and 2 can be ignored.[47] Therefore Eq. 1 can be substituted in Eq. 2 as follows to calculate the magnitude of the electrical field,

$$|\mathbf{E}| \approx -\frac{\partial V}{\partial r} = \frac{\rho r}{3\varepsilon_0} \quad (3)$$

To gain further insight into the electrospray deposition, various forces exerting on a charged droplet moving through still air, with an imposed electrical field, were examined, including electrostatic force, gravitational and buoyancy

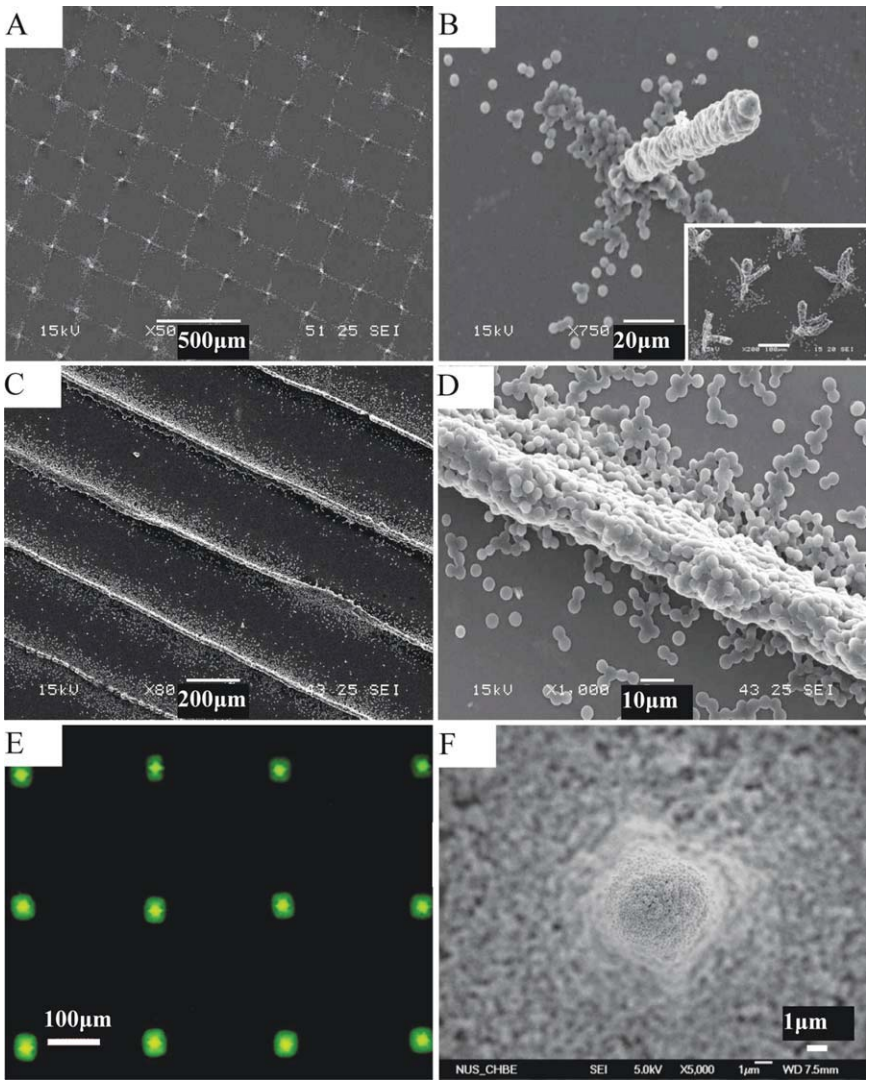

Figure 9. (A–D) Three-dimensional PLGA particle micropattern formation.

Scale bar for the inset in (B) is 100 μm. (E) Fluorescence microscopy image of FITC-PS nanoparticles pattern. (F) SEM image illustrating high magnified view of (E). [Color figure can be viewed in the online issue, which is available at wileyonlinelibrary.com.]

forces, drag force due to air resistance, columbic repulsion force, and image force. Charges of individual droplets in a positive-ion electrospray of pure acetonitrile near the Rayleigh limit of charge were measured.[48] Here, the maximum charge on the droplet generated by electrospray can be estimated by Rayleigh equation:

$$q_d = 8\pi(\varepsilon_0 \gamma R_d^3)^{1/2} \tag{4}$$

where q_d is the charge, ε_0 is the electrical permittivity of vacuum, γ is the surface tension, and $\boldsymbol{R}_d$ is the radius of droplet. The magnitude of the electric field force (F_E) can be calculated by the following equation.

$$F_E = |\mathbf{E}|q_d \tag{5}$$

The magnitude of the gravitational (F_g) and buoyancy (F_B) forces can be incorporated into each other and calculated by Eq. 6.

$$F_g + F_B = \frac{4}{3}\pi R_d^3(\rho_d - \rho_f)g \tag{6}$$

where ρ_d is the density of droplet, ρ_f is the density of fluid, and g is the magnitude of the gravitational acceleration. The magnitude of the electrical force between the droplets and the induced charge on the conductive grounded plate (which is named as the image force, F_{im}) can be calculated by the following equation.

$$F_{im} = \frac{q^2}{2\pi\varepsilon_0 a^3}\frac{r}{\left[1-(r/a)^2\right]^2} \tag{7}$$

Equation 7 is mentioned in spherical coordinates, where a shows the distance between the droplet and the substrate surface and r shows the droplet position in the r-direction.[49]

The magnitude of the columbic repulsion force vector (F_q) can be calculated by Eq. 8.

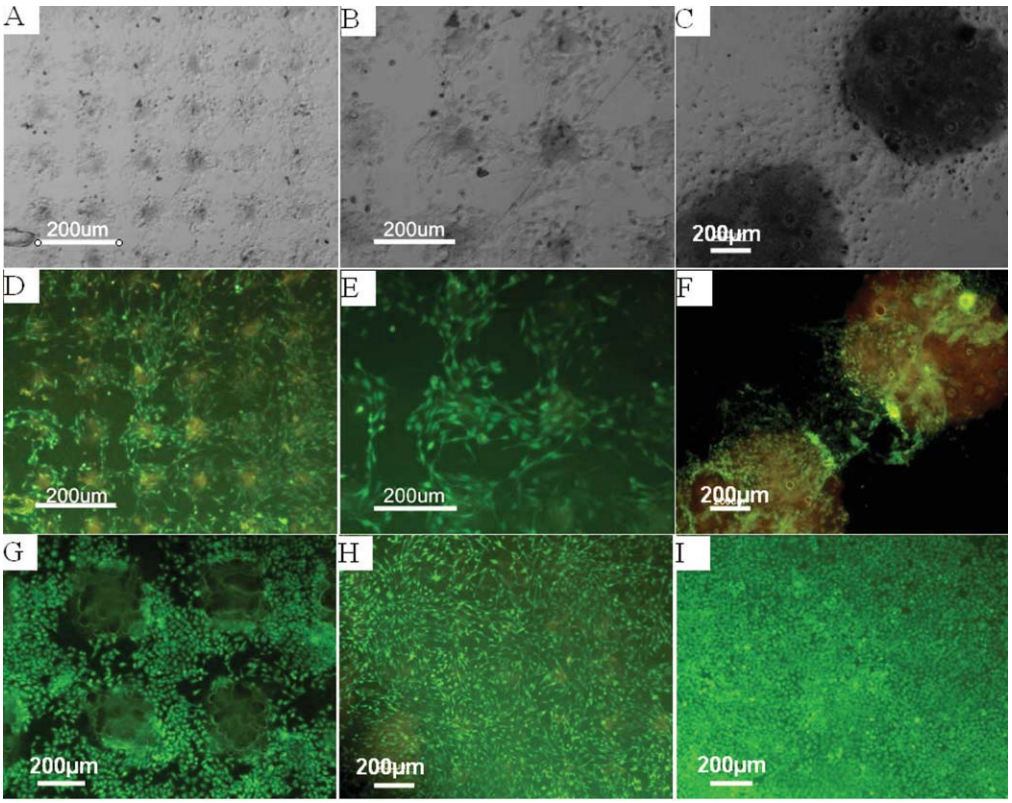

Figure 10. (A–C) Optical phase contrast microscopy images indicating cell pattern formation after the generation of particle pattern on the plastic substrate incubated with Hep G2 cells for 3 days and the regions without particle deposition being coated with pluronic F127; (D–F) Fluorescent microscopy images corresponding to A–C (green color indicates the living cells stained with FDA); (G) PLGA particle pattern on the glass slide with the adsorption of pluronic F127 on the surface of PLGA particle pattern; (H) PLGA particle pattern on the plastic slide without the coating of pluronic F127; (I) plastic slide substrate without particle pattern.

The particle patterns were prepared with a feed rate of 3 ml/h for 5% PLGA DCM solution. [Color figure can be viewed in the online issue, which is available at wileyonlinelibrary.com.]

$$F_{\mathrm{q}} = \sum_{i=2}^{n} \frac{q \cdot q_i}{4\pi\varepsilon_0} \frac{1}{r_i^2} \tag{8}$$

where r_{i} shows the center–center distance between the droplet of concern and surrounding droplets. The magnitude of the drag force (F_D) can be estimated by the following equation.

$$F_{\mathrm{D}} = \frac{1}{2} C_{\mathrm{D}} (\pi R_{\mathrm{d}}^2) \rho_{\mathrm{f}} u_{\upsilon}^2 \tag{9}$$

where u_{υ} is the droplet velocity due to the drag and gravitational forces, πR_{d}^2 is the cross sectional area perpendicular to the flow direction, and C_{D} is the drag coefficient. The velocity of droplets ($\approx$0.23 $\pm$ 0.13 m/s) under the representative fabrication parameter set was determined by Phase Doppler Particle Analyzer (TSI Inc. MN) at the position of 3 cm below the tip of nozzle, with the characteristic Reynolds number corresponding to the Stoke's regime ($Re \approx 0.001$–0.4). Drag coefficient in Stock's regime can be calculated by the following equation.

$$C_{\mathrm{D}} = \frac{24}{\mathrm{Re}} = \frac{12\mu}{\rho_{\mathrm{f}} u_{\upsilon} R_{\mathrm{d}}} \tag{10}$$

Therefore, Eq. 10 can be substituted in Eq. 9 and results in the following equation.

$$F_{\mathrm{D}} = 6\pi\mu R_{\mathrm{d}} u_{\upsilon} \tag{11}$$

Electrical charge on droplets can easily be represented by space charge density using the following equation.

$$\rho = \frac{q}{\frac{4}{3}\pi R_{\mathrm{d}}^3} \tag{12}$$

where ρ is the space charge density. The force balance equation for falling droplet can be developed as follows

$$\rho_{\mathrm{d}} \left(\frac{4}{3} \pi R_{\mathrm{d}}^3 \right) \frac{du}{dt} = F_{\mathrm{D}} + F_{\mathrm{E}} + F_{\mathrm{g}} + F_{\mathrm{B}} + F_{\mathrm{q}} + F_{\mathrm{im}} \tag{13}$$

where u is the total velocity, which can be considered as sum of the two velocities, the velocity of the charged droplets due to the drag and gravitational forces, u_υ and the velocity of the charged droplets due to the electrical forces, u_e. Thus, Eq. 13 can be rewritten as follows

$$\rho_d\left(\frac{4}{3}\pi R_d^3\right)\frac{d(u_\upsilon+u_e)}{dt}=\rho_d\left(\frac{4}{3}\pi R_d^3\right)\left[\frac{du_\upsilon}{dt}+\frac{du_e}{dt}\right]$$
$$=F_D+F_E+F_g+F_B+F_q+F_{im} \quad (14)$$

After substituting Eq. 3 to 12 in Eq. 14, it can be divided in two separate equations as follows

$$\rho_d\left(\frac{4}{3}\pi R_d^3\right)\frac{du_\upsilon}{dt}=6\pi\mu R_d u_\upsilon+\frac{4}{3}\pi R_d^3(\rho_d-\rho_f)g \quad (15)$$

$$\rho_d\left(\frac{4}{3}\pi R_d^3\right)\frac{du_e}{dt}=\left(\frac{4}{3}\pi R_d^3\right)\frac{\rho^2 r}{3\varepsilon_0}+\left(\frac{4}{3}\pi R_d^3\right)^2\frac{\rho^2}{4\pi\varepsilon_0}\sum_{i=2}^{n}\frac{1}{r_i^2}$$
$$+\left(\frac{4}{3}\pi R_d^3\right)^2\frac{\rho^2}{2\pi\varepsilon_0 a^3}\frac{r}{\left[1-(r/a)^2\right]^2} \quad (16)$$

An additional equation is needed to describe the charge variation on the droplet. Therefore, the equation of charge conservation can be used. The general form of this equation can be written as.[50]

$$\frac{\partial\rho}{\partial t}+\nabla.\mathbf{J}=0 \quad (17)$$

In this equation, $\mathbf{J}$ shows the current density vector in the unit of $Cm^{-2}s^{-1}$, which can be calculated by the following equation.[50]

$$\nabla.\mathbf{J}=-D\nabla^2\rho+\mathbf{u}.\nabla\rho+\frac{b\rho^2}{\varepsilon_0}$$
$$=-D\nabla^2\rho+(\mathbf{u}_\upsilon+\mathbf{u}_e).\nabla\rho+\frac{b\rho^2}{\varepsilon_0} \quad (18)$$

where $\mathbf{u}$, $\mathbf{u}_\upsilon$, and $\mathbf{u_e}$ are the total velocity vector, the velocity vector of the charged droplets due to the drag and gravitational forces and the velocity vector of the charged droplets due to the electrical forces, respectively. In addition, D and b are the mean charge species molecular diffusion coefficient and the electrical charge species mobility, respectively.[50] The electrical charge species mobility can be calculated by the following equation.

$$b=\frac{u_e}{E}=\frac{K}{\rho} \quad (19)$$

where K is the electrical conductivity. Below is a list of notable features in Eq. 18.

$D\nabla^2\rho$ is the molecular diffusion term for the charged species.

$u_\upsilon\nabla\rho$ is the convection term of the charged species due to the drag and gravitational forces.

$u_e\nabla\rho$ is the convection term of the charged species due to the electrical field.

$\frac{b\rho^2}{\varepsilon_0}$ refers to the motion of the charged species due to the repulsion of charged species of the same polarity.

Substituting Eqs 18 and 19 in Eq. 17, results in the following equation.

$$\frac{\partial\rho}{\partial t}=D\nabla^2\rho-(\mathbf{u}_\upsilon+\mathbf{u}_e).\nabla\rho-\frac{K}{\varepsilon_0}\rho \quad (20)$$

Equation 20 can be rewritten as follows if the variations in θ and ϕ directions are ignored.

$$\frac{\partial\rho}{\partial t}=D\frac{\partial^2\rho}{\partial r^2}-(\mathbf{u}_\upsilon+\mathbf{u}_e).\frac{\partial\rho}{\partial r}-\frac{K}{\varepsilon_0}\rho \quad (21)$$

Therefore, the following equations can be considered as the governing equations in a scalar form.

$$\rho_d\left(\frac{4}{3}\pi R_d^3\right)\frac{du_\upsilon}{dt}=6\pi\mu R_d u_\upsilon+\frac{4}{3}\pi R_d^3(\rho_d-\rho_f)g \quad (22)$$

$$\rho_d\left(\frac{4}{3}\pi R_d^3\right)\frac{du_e}{dt}=\left(\frac{4}{3}\pi R_d^3\right)\frac{\rho^2 r}{3\varepsilon_0}+\left(\frac{4}{3}\pi R_d^3\right)^2\frac{\rho^2}{4\pi\varepsilon_0}\sum_{i=2}^{n}\frac{1}{r_i^2}$$
$$+\left(\frac{4}{3}\pi R_d^3\right)^2\frac{\rho^2}{2\pi\varepsilon_0 a^3}\frac{r}{\left[1-(r/a)^2\right]^2} \quad (23)$$

$$\frac{\partial\rho}{\partial t}=D\frac{\partial^2\rho}{\partial r^2}-(u_\upsilon+u_e).\frac{\partial\rho}{\partial r}-\frac{K}{\varepsilon_0}\rho \quad (24)$$

Initial and Boundary Conditions. To complete the model specification, three initial conditions and two boundary equations are required. The initial conditions for velocities and space charge density are given by:

$$u_\upsilon=0 \quad \text{at} \quad t=0 \quad (25)$$

$$u_e=0 \quad \text{at} \quad t=0 \quad (26)$$

$$\rho=0 \quad \text{at} \quad t=0 \quad (27)$$

The boundary conditions for space charge density are as follows

$$\rho=6\left(\varepsilon_0\gamma R_d^{-3}\right)^{\frac{1}{2}} \quad \text{at} \quad r=R_d \quad (28)$$

$$\rho=0 \quad \text{at} \quad r=R_0 \quad (29)$$

The maximum charge calculated by Rayleigh Equation (Eq. 4) is used for defining the boundary condition on the particle surface. R_0 (= $2R_d$) is the radius of the imaginary periphery around the droplet (Figure 11) in which the effect

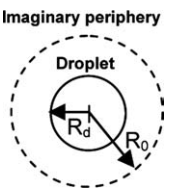

Figure 11. Geometry for the scaling analysis.

of neighboring droplets are significant. In fact, the considered droplet is an isolated droplet when there is not any other droplet within the imaginary periphery. An isolated droplet does not have any interaction with the other droplets. The sensitive analysis for the general case $R_0 = xR_d$ ($x > 1$), will be discussed under the "Results and Discussion" section.

Scaling Analysis. Scaling analysis, as described by Krantz and Sczechowski[51]and Krantz[52,53] is used to assess the relative importance of the various forces in force balance equations. The subject of scaling analysis deals with a systematic method for non-dimensionalizing a system of governing equations. The resulting dimensionless system of equations illustrates the minimum parametric representation (MPR) of the process. In this method, the magnitude of the particular dimensionless variable or its derivative is bounded between zero and more-or-less one, O(1).[53] Therefore, the values of the dimensionless groups can determine the significance of various terms multiplying them. For instance, if a dimensionless group is of order 0.01, O(0.01), or less, the term that it multiplies can be ignored. Hence, by using scaling analysis, one can appropriately simplify the governing equations of a process and elucidate system behavior without any rigorous simulation. A proper scaling analysis can reduce the describing equations for a physical process to their minimum parametric form, i.e., in terms of the minimum number of dimensionless groups. These resulting dimensionless groups permit assessing the relative importance of the terms in the equation.[51–53,54] As the criteria emanating from scaling analysis are not system-specific, it permits assessing the importance of the considered terms in general. We define the following dimensionless variables:

$$u_v^* \equiv \frac{u_v}{u_{vs}}; u_e^* \equiv \frac{u_e}{u_{es}}; r^* \equiv \frac{r - r_r}{r_s}; \rho^* \equiv \frac{\rho}{\rho_s}; t^* \equiv \frac{t}{t_s} \tag{30}$$

where the subscripts s and r denote scale factor and reference factor, respectively, and the superscript "*" refers to a dimensionless variable. Scale factors are introduced to make the dimensionless variables of O(1), while reference factors are introduced to bound the dimensionless variables to be between zero and one. Indeed, for the variables that are not referenced to zero in the initial and boundary conditions, an unspecified reference factor is included. These dimensionless variables are introduced into Eqs. 22–29 to obtain the corresponding dimensionless governing equations.

$$\frac{2\rho_d R_d^2}{9t_s\mu}\frac{du_v^*}{dt^*} = u_v^* + \frac{2R_d^2(\rho_d - \rho_f)g}{9\mu u_{vs}} \tag{31}$$

$$\frac{3\rho_d u_{es}\varepsilon_0}{t_s\rho_s^2 r_s}\frac{du_e^*}{dt^*} = \rho^{*^2} r^* + \frac{R_d^3}{r_s}\rho^{*^2}\sum_{i=2}^{n}\frac{1}{r_i^2} + \frac{2(R_d^3)}{a^3}\frac{r^*\rho^{*^2}}{\left[1 - \left(\frac{r_s}{a}\right)^2 r^{*^2}\right]^2} \tag{32}$$

$$\frac{\varepsilon_0}{Kt_s}\frac{\partial\rho^*}{\partial t^*} = \frac{D\varepsilon_0}{Kr_s^2}\frac{\partial^2\rho^*}{\partial r^{*^2}} - \left(\frac{u_{vs}\varepsilon_0}{Kr_s}u_v^* + \frac{u_{es}\varepsilon_0}{Kr_s}u_e^*\right)\frac{\partial\rho^*}{\partial r^*} - \rho^* \tag{33}$$

$$u_v^* = 0 \quad \text{at} \quad t^* = 0 \tag{34}$$

$$u_e^* = 0 \quad \text{at} \quad t^* = 0 \tag{35}$$

$$\rho^* = 0 \quad \text{at} \quad t^* = 0 \tag{36}$$

$$\rho^* = \frac{6\left(\varepsilon_0\gamma R_d^{-3}\right)^{\frac{1}{2}}}{\rho_s} \quad \text{at} \quad r^* = \frac{R_d - r_r}{r_s} \tag{37}$$

$$\rho^* = 0 \quad \text{at} \quad r^* = \frac{R_0 - r_r}{r_s} \tag{38}$$

The radial length scale and reference factors are obtained from the dimensionless groups in Eqs. 37 and 38

$$\frac{R_d - r_r}{r_s} = 0 \Rightarrow r_r = R_d \tag{39}$$

$$\frac{R_0 - r_r}{r_s} = \frac{R_0 - R_d}{r_s} = 1 \Rightarrow r_s = R_0 - R_d = R_d \tag{40}$$

Similarly, the velocity scale factors can be obtained using the dimensionless groups in Eqs. 31 and 33.

$$\frac{2R_d^2(\rho_d - \rho_f)g}{9\mu u_{vs}} = 1 \Rightarrow u_{vs} = \frac{2R_d^2(\rho_d - \rho_f)g}{9\mu} \tag{41}$$

$$\frac{u_{es}\varepsilon_0}{Kr_s} = 1 \Rightarrow u_{es} = \frac{KR_d}{\varepsilon_0} \tag{42}$$

The scale factor for space charge density can be obtained using Eq. 37.

$$\frac{6\left(\varepsilon_0\gamma R_d^{-3}\right)^{\frac{1}{2}}}{\rho_s} = 1 \Rightarrow \rho_s = 6\left(\varepsilon_0\gamma R_d^{-3}\right)^{\frac{1}{2}} \tag{43}$$

Another scale factor that should be taken into account is the time scale. The most general time scale is the instantaneous time at which the process is observed; this time scale is called "the observation time," t_o. Clearly, $0 \geq t_o > \infty$ since this scale is the actual time commencing from the inception of the unsteady-state process.[53]

The mentioned scale and reference factors result in the following set of dimensionless governing equations, which constitute the minimum parametric representation:

$$\frac{2\rho_d R_d^2}{9t_o\mu}\frac{du_v^*}{dt^*} = u_v^* + 1 \tag{44}$$

$$\frac{\rho_d K R_d^3}{12t_o\varepsilon_0\gamma}\frac{du_e^*}{dt^*} = \rho^{*^2} r^* + R_d^2\sum_{i=2}^{n}\frac{1}{r_i^2}\rho^{*^2} + \frac{2\left(R_d^3\right)}{a^3}\frac{r^*\rho^{*^2}}{\left[1 - \left(\frac{R_d}{a}\right)^2 r^{*^2}\right]^2} \tag{45}$$

$$\frac{\varepsilon_0}{Kt_o}\frac{\partial\rho^*}{\partial t^*} = \frac{D\varepsilon_0}{KR_d^2}\frac{\partial^2\rho^*}{\partial r^{*^2}} - \left[\frac{2R_d(\rho_d - \rho_f)g\varepsilon_0}{9\mu K}u_v^* + u_e^*\right]\frac{\partial\rho^*}{\partial r^*} - \rho^* \tag{46}$$

$$u_v^* = 0 \quad \text{at} \quad t^* = 0 \tag{47}$$

$$u_e^* = 0 \quad \text{at} \quad t^* = 0 \tag{48}$$

$$\rho^* = 0 \quad \text{at} \quad t^* = 0 \tag{49}$$

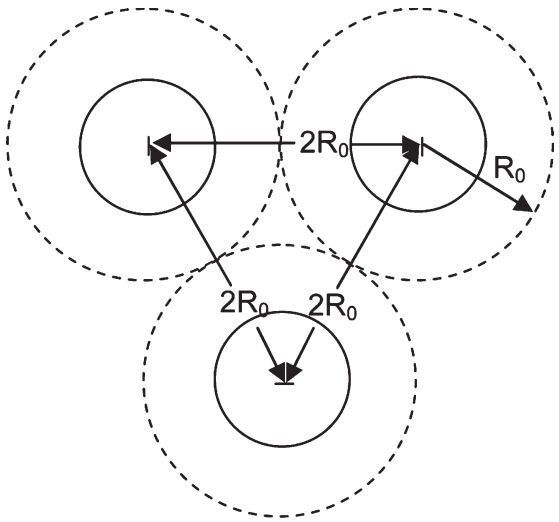

Figure 12. Interparticle spacing.

$$\rho^* = 1 \quad \text{at} \quad r^* = 0 \tag{50}$$

$$\rho^* = 0 \quad \text{at} \quad r^* = 1 \tag{51}$$

The mentioned dimensionless governing equations can be used to determine the time needed to reach a steady-state. Hence, the coefficient of the unsteady-state term in each equation should be as small as possible. For instance, for Eq. 44:

$$\frac{2\rho_d R_d^2}{9t_0\mu} \ll 1 \Rightarrow t_0 \gg \frac{2\rho_d R_d^2}{9\mu} = \frac{\rho_d d^2}{18\mu} = t_{sv} \tag{52}$$

where d is droplet diameter. The time scale represented in Eq. 52 can be defined as "the momentum response time," t_{sv}. The momentum response time shows the time required for a particle to respond to a change in velocity due to the change in drag and gravitational force.[55]

Similarly, for Eq. 45

$$\frac{\rho_d K R_d^3}{12t_0\varepsilon_0\gamma} \ll 1 \Rightarrow t_0 \gg \frac{\rho_d K R_d^3}{12\varepsilon_0\gamma} = t_{se} \tag{53}$$

The time scale represented in Eq. 53 can be defined as "the electrical response time," t_{se}.

"The electrical response time" shows the time required for a particle to respond to a change in velocity due to the change in each type of electrical forces.[55] The time scales defined in Eqs. 52 and 53 permit us to determine the criteria for assuming that the transients associated with fluid and particle interaction induced during start-up of the process have died out.

The last time scale can be found from Eq. 46.

$$\frac{\varepsilon_0}{Kt_0} \ll 1 \Rightarrow t_0 \gg \frac{\varepsilon_0}{K} = t_{s\rho} \tag{54}$$

The time scale in Eq. 54 is known as "the electrical relaxation time,"[53] $t_{s\rho}$, which is used to define the charge relaxation time in the system.

A triangle pattern is considered for the droplets in neighborhood which is shown in Figure 12. For simplicity we can assume that there are n droplets with equal separation ($d_0 = 2R_0$) surrounding the particular droplet of concern.

Considering the points mentioned above, the four time-independent dimensionless groups appearing in Eqs. 45 and 46 are summarized below:

$$N_1 = R_d^2 \sum_{i=2}^{n} \frac{1}{r_i^2} = n\frac{R_d^2}{d_0^2} \tag{55}$$

$$N_2 = \frac{2\left(R_d^3\right)}{a^3} \tag{56}$$

$$N_3 = \frac{D\varepsilon_0}{KR_d^2} \tag{57}$$

$$N_4 = \frac{2R_d(\rho_d - \rho_f)g\varepsilon_0}{9\mu K} \tag{58}$$

It is note worthy that N_1, N_2, N_3, and N_4 are the coefficients for the columbic repulsion force term, the image force term, the molecular diffusion term and the convection of the charged species term due to the drag and gravitational forces, respectively.

N_1 can be related to volume fraction of the particle as dispersed phase in continuous phase (α_d),

$$\alpha_d = \frac{\text{Volume of the dispersed phase}}{\text{Volume of the continuous phase}} = \frac{\frac{4}{3}\pi R_d^3}{\frac{\pi}{6}d_0^3} = 8\frac{R_d^3}{d_0^3} \tag{59}$$

Using Eq. 59, N_1 can be rewritten as follows,

$$N_1 = n\frac{R_d^2}{d_0^2} = \frac{n}{4}\alpha_d^{2/3} \tag{60}$$

The mentioned dimensionless groups were evaluated based on the physical and geometrical properties of the dispersed and continuous phases given in Table 1 and are summarized in Table 2.

Since $N_1 \ll 1$, the columbic repulsion force term in Eq. 45 can be neglected. Similarly, since $N_2 \ll 1$, the image force term in Eq. 45 has a negligible effect. In the same way, since $N_3 \ll 1$ and $N_4 \ll 1$, the molecular diffusion

Table 1. Physical and Geometrical Parameters for the Particle Deposition System

Property	Value
Droplet radius (R_d)	10^{-6} (m)
Droplet density (ρ_d)	1200 (kg/m^3)
Air density (ρ_f)	1.5 (kg/m^3)
Air electrical conductivity (K)	0.0262 (C^2 s/kg m^3)
Air permittivity (ε_0)	8.85×10^{-12} (C^2 s^2/kg m^3)
Molecular diffusivity (D)	10^{-5} (m^2/s)
Air viscosity (μ)	1.85×10^{-5} (kg/m s)
Gravity acceleration (g)	9.8 (m/s^2)
Distance between particle and collecting plate (a)	0.000005 (m)
Number of particles (n)	1000

Table 2. Characteristic Dimensionless Groups for the Particle Deposition Process

Dimensionless Groups	Value
N_1	5.2×10^{-5}
N_2	2×10^{-3}
N_3	3.4×10^{-3}
N_4	4.8×10^{-8}

term and the convection of the charged species term due to the drag and gravitational forces in Eq. 46 also can be neglected.

Debye Length. Interestingly, if $t_{sv} < t_{s\rho}$, the effect of the space charge will be confined to a region-of-influence around the particle which can be shown by δ_ρ and is equal to $R_0 - R_d$ (known as r_s). In fact, this region is a boundary layer around the particle which is called "Debye length." This length can be obtained using the dimensionless group in Eq. 57. N_3 should be set equal to one to consider the effect of the molecular diffusion term on the charge variation.

$$N_3 = \frac{D\varepsilon_0}{Kr_s^2} = \frac{D\varepsilon_0}{K\delta_\rho^2} = 1 \Rightarrow \delta_\rho = \sqrt{Dt_{s\rho}} \tag{61}$$

It should be noted that the above analysis was performed under the special condition $R_0 = 2R_d$ as an illustration in the scaling analysis. We have performed a separate sensitivity analysis on the variation of x, given $R_0 = xR_d$ ($x > 1$). The corresponding results show that it will not make a considerable difference from the typical scaling analysis results if we consider $x > 1$ (data not shown).

Conclusions

In summary, we have demonstrated that a simple (single step) yet versatile and robust approach (a combination of top-down approach for formation of particles from bulk material and bottom-up approach for the generation of structure and pattern from the particles mentioned earlier) to generate biodegradable polymeric particle micropatterns on a substrate using electric field controlled electrospray deposition through a mask. Particle size can be controlled by adjusting processing parameters and physical properties of the solution. The features of particle patterns could be tailored using different masks. Furthermore, cell patterns can be achieved on the surface of particle patterns by blocking the areas without particle deposition on the substrate and culturing cells on the substrate. Transfected cell microarrays as a complementary technique to DNA microarrays and protein microarrays have been developed as a method for gene product screening.[56–58] In view of this, electrospray deposition could be used to encapsulate DNA plasmids and cell adhesive materials in polymeric particles. Moreover, such systems could as well serve as controlled release systems of DNA plasmids from particles to transfect cells on the surface of particles to form transfected cell array for future studies. A model has been also developed to describe the particle deposition process. Scaling analysis was used to show that both columbic repulsion force between the particles and image force between the particles and substrate surface can be ignored.

Acknowledgments

This project has been supported by the Singapore Science and Engineering Research Council (SERC) and National University of Singapore under the grant number R279-000-208-305. The authors thank Dr. Lai Yeng Lee, Liang Kuang Lim, and Sudhir Hulikal Ranganath for their technical support on this work.

Literature Cited

1. Fadiel A, Naftolin F. Microarray applications and challenges: a vast array of possibilities. *Int Arch Biosci*. 2003;1:111–1121.
2. Whitesides GM, Ostuni E, Takayama S, Jiang X, Ingber DE. Soft lithography in biology and biochemistry. *Annu Rev Biomed Eng*. 2001;3:335–373.
3. Sanjana NE, Fuller SB. A fast flexible ink-jet printing method for patterning dissociated neurons in culture. *J Neurosci Methods*. 2004;136:151–163.
4. Geissler M, Xia Y. Patterning: principles and some new developments. *Adv Mater*. 2004;16:1249–1269.
5. Falconnet D, Csucs G, Grandin HM, Textor M. Surface engineering approaches to micropattern surfaces for cell-based assays. *Biomaterials*. 2006;27:3044–3063.
6. Khademhosseini A, Langer R. Nanobiotechnology drug delivery and tissue engineering, Nanobiotechnology—drug delivery and tissue engineering. *Chem Eng Prog*. 2006;102:38–42.
7. Raghavan S, Chen CS. Micropatterned environments in cell biology. *Adv Mater*. 2004;16:1303–1313.
8. Folch A, Toner M. Microengineering of cellular interactions. *Annu Rev Biomed Eng*. 2000;2:227–256.
9. Nishizawa M, Takoh K, Matuse T. Micropatterning of HeLa cells on glass substrates and evaluation of respiratory activity using microelectrodes. *Langmuir*. 2002;18:3645–3649.
10. Hyun J, Ma H, Zhang Z, Beebe TP, Chilkoti A. Universal route to cell micropatterning using an amphiphilic comb polymer. *Adv Mater*. 2003;15:576–579.
11. Pal R, Sung KE, Burns MA. Microstencils for the patterning of non-traditional materials. *Langmuir*. 2006;22:5392–5397.
12. Morozov VN, Morozova TY. Electrospray deposition as a method for mass fabrication of mono- and multicomponent microarrays of biological and biologically active substances. *Anal Chem*. 1999;71:3110–3117.
13. Velev OD, Kaler EW. In situ assembly of colloidal particles into miniaturized biosensors. *Langmuir*. 1999;15:3693–3698.
14. Yeh S, Seul M, Shraiman BI. Assembly of ordered colloidal aggregates by electric-field-induced fluid flow. *Nature*. 1997;386:57–59.
15. Kim E, Xia YN, Whitesides GM. Two- and three-dimensional crystallization of polymeric microspheres by micromolding in capillaries. *Adv Mater*. 1996;8:245–247.
16. Hayward RC, Saville DA, Aksay IA. Electrophoretic assembly of colloidal crystals with optically tunable micropatterns. *Nature*. 2000;404:56–59.
17. Trau M, Saville DA, Aksay IA. Field-induced layering of colloidal crystals. *Science*. 1996;272:706–709.
18. Huang J, Tao AR, Connor S, He R, Yang P. A general method for assembling single colloidal particle lines. *Nano Lett*. 2006;6:524–529.
19. Huang J, Kim F, Tao AR, Connor S, Yang P. Dewetting induced formation of ordered nanoparticle stripe patterns. *Nature Mater*. 2005;4:896–900.
20. Buchko CJ, Kozloff KM, Sioshansi A, O'shea KS, Martin DC. Electric field mediated deposition of bioactive polypeptides on neural prosthetic devices. *Mater Res Soc Symp Proc*. 1996;414:23.
21. Li X, Edirisinghe M. Novel patterning of nano-bioceramics: template-assisted Electrohydrodynamic atomization spraying. *J R Soc Interface*. 2008;5:253–257.
22. Li X, Koller G, Huang J, Silvio LD, Renton T, Esat M, Bonfield W, Edirisinghe M. A novel jet-based nano-bioceramic patterning technique for osteoblast guidance. *J R Soc Interface*. 2010;7:189–197.

23. Ahmad Z, Nangrejo M, Edirisinghe M, Stride E, Colombo P, Zhang HB. Engineering a material for biomedical applications with electric field assisted process. *Appl Phys A*. 2009;97:31–37.
24. Avseenko NV, Morozova TY, Ataullakhanov FI, Morozov VN. Immobilization of proteins in immunochemical microarrays fabricated by electrospray deposition. *Anal Chem*. 2001;73:6047–6052.
25. Avseenko NV, Morozova TY, Ataullakhanov FI, Morozov VN. Immunoassay with multicomponent protein microarrays fabricated by electrospray deposition. *Anal Chem*. 2002;74:927–933.
26. Kim J, Yamagata Y, Takasaki M, Lee B, Ohmori H, Higuchi T. A device for fabricating protein chips by using a surface acoustic wave atomizer and electrostatic deposition. *Sens Acuators B*. 2005;107: 535–545.
27. Chen CH, Kelder EM, Vanderput PJJM, Schoonman JJ. Morphology control of thin $LiCoO_2$ films fabricated using the electrostatic spray deposition (ESD) technique. *Mater Chem.* 1996;6:765–771.
28. Lapham DP, Colbeck I, Schoonman J, Kamlag Y. The preparation of $NiCo_2O_4$ films by electrostatic spray deposition. *Thin Solid Films*. 2001;391:17–20.
29. Peng M, Balachandran W, Xiao P. Formation of ceramic thin films using electrospray in cone-jet mode. *IEEE Trans Ind Appl*. 2002;38:50–56.
30. Sanders EH, McGrady KA, Wnek GE, Edmondson CA, Mueller JM, Fontanella JJ, Suarez S, Greenbaum SG. Characterization of electrosprayed Nafion films. *J Power Sources*. 2004;129:55–61.
31. Pareta R, Edirisinghe MI. A novel method for the preparation of starch films and coatings. *Carbohydr Polym*. 2006;63:425–431.
32. Uematsu I, Matsumoto H, Morota K, Minagawa M, Tnanioka A, Yamagata Y, Inoue K. Surface morphology and biological activity of protein thin films produced by electrospray deposition. *J Colloid Inter Sci*. 2004;269:336–340.
33. Morozov VN, Morozova TY. Electrospray deposition as a method to fabricate functionally active protein films. *Anal Chem*. 1999;71: 1415–1420.
34. Lee B, Kamiya N, Machida S, Yamagata Y, Horie K, Nagamune T. Fabrication of a protein film by electrospray deposition method and investigation of photochemical properties by persistent spectral hole burning. *Biomaterials*. 2003;24:2045–2051.
35. Hoyer B, Sorensen G, Jensen N, Nielsen DB, Larsen B. Electrostatic spraying: a novel technique for preparation of polymer coatings on electrodes. *Anal Chem*. 1996;68:3840–3844.
36. Rietveld IB, Kobayashi K, Yamada H, Matsushige K. Morphology control of poly(vinylidene fluoride) thin film made with electrospray. *J Colloid Interface Sci*. 2006;298:639–651.
37. Saf R, Goriup M, Steindl T, Hamedinger TE, Sandholzer D, Hayn G. Thin organic films by atmospheric-pressure ion deposition. *Nature Mater*. 2004;3:323–329.
38. Lenggoro IW, Lee HM, Okuyama K. Nanoparticle assembly on patterned "plus/minus" surfaces from electrospray of colloidal dispersion. *J Colloid Interface Sci*. 2006;303:124–130.
39. Kim H, Kim J, Yang H, Suh J, Kim T, Han B, Kim S, Kim DS, Pikhitsa PV, Choi M. Parallel patterning of nanoparticles via electrodynamic focusing of charged aerosols. *Nat Nanotechnol*. 2006;1: 117–121.
40. Xie J, Marijnissen JCM, Wang CH. Microparticles developed by electrohydrodynamic atomization (EHDA) for the local delivery of anticancer drug to treat C6 glioma in vitro. *Biomaterials*. 2006;27: 3321–3332.
41. Xie J, Lim LK, Phua YY, Hua JS, Wang CH. Electrohydrodynamic atomization for biodegradable polymeric particle production. *J Colloid Interface Sci*. 2006;302:103–112.
42. Xie J, Wang CH. Encapsulation of proteins in biodegradable polymeric microparticles using electrospray in the Taylor cone-jet mode. *Biotechol Bioeng*. 2007;97:1278–1290.
43. Roh K, Martin DC, Lahann J. Biphasic Janus particles with nanoscale anisotropy. *Nat Mater*. 2005;4:759–763.
44. Roh K, Martin DC, Lahann J. Triphasic nanocolloids. *J Am Chem Soc*. 2006;128:6796–6797.
45. Fonzo FD, Gidwani A, Fan MH, Neumann D, Iordanoglou DI, Heberlein JVR, McMurry PH, Girshick SL, Tymiak N, Gerberich WW. Focused nanoparticle-beam deposition of patterned microstructures. *Appl Phys Lett*. 2000;77:910–912.
46. Liu VA, Jastromb WE, Bhatia SN. Engineering protein and cell adhesivity using PEO-terminated triblock polymers. *J Biomed Mater Res*. 2002;60:126–134.
47. Bailey AG. *Electrostatic Spraying of Liquids*. Great Britain: Research Studies Press, 1988.
48. Smith JN, Flagan RC, Beauchamp JL. Droplet evaporation and discharge dynamics in electrospray ionization. *J Phys Chem A*. 2002; 106:9957–9967.
49. Tinkle MD, Barlow SE. Image charge forces inside conducting boundaries. *J Appl Phys*. 2001;90:1612–1624.
50. Sigmond RS. Simple approximation treatment of unipolar space-charge-dominated coronas: the Warburg law and saturation current. *J Appl Phys*. 1982;53:891–898.
51. Krantz WB, Sczechowski JG. Scaling initial and boundary value problems: a tool in engineering teaching and practice. *Chem Eng Educ*. 1994;28:236–253.
52. Krantz WB. An alternative method for teaching and implementing dimensional analysis. *Chem Eng Educ*. 2000;34:216–221.
53. Krantz WB. *Scaling Analysis in Modeling Transport and Reaction Processes*. New York: Wiley, 2007.
54. Kopaygorodsky EM, Krantz WB, Guliants VV. Scaling analysis-a valuable technique in engineering teaching and practice. *Presented at the American Society for Engineering Education Annual Conference and Exposition*, Albuquerque, NM, 2001.
55. Crown C, Sommerfeld M, Tsuji Y. *Multiphase Flows with Droplets and Particles*. USA: CRC, 1998.
56. Ziauddin J, Sabatini DM. Microarrays of cells expressing defined cDNAs. *Nature*. 2001;411:107–110.
57. Bailey SN, Wu RZ, Sabatini DM. Applications of transfected cell microarrays in high-throughput drug discovery. *Drug Discov Today*. 2002;7:1–6.
58. Wu RZ, Bailey SN, Sabatini DM. Cell-biological applications of transfected-cell microarrays. *Trends Cell Biol*. 2002;12:485–488.

Manuscript received July 31, 2009, and revision received Dec. 21, 2009.